buildings

MDPI

Article

Influence of Porous Structure of Non-Autoclaved Bio-Based Foamed Concrete on Mechanical Strength

Abdelrahman Mohamad [1], Fouzia Khadraoui [1,*], Daniel Chateigner [2] and Mohamed Boutouil [1]

[1] Builders Lab, Builders Ecole d'Ingénieurs, ComUE Normandie Université, 1 Rue Pierre et Marie Curie, 14610 Epron, France; mohamed.boutouil@builders-ingenieurs.fr (M.B.)
[2] CRISMAT, CNRS UMR 6508, ENSICAEN, IUT Grand-Ouest Normandie, Université de Caen Normandie, Normandie Université, 6 Bd Maréchal Juin, CEDEX 4, 14050 Caen, France; daniel.chateigner@ensicaen.fr
* Correspondence: fouzia.khadraoui-mehir@builders-ingenieurs.fr

Abstract: This study examines the impact of the porous structure on the density and mechanical behavior of a new foamed concrete incorporating hemp shives. The specific aim is to gain a better understanding of how the inclusion of hemp shiv, as well as different additions and foaming methods, influence the density and mechanical strength of the concrete. A total of eight batches of foam concrete were produced and tested, made with a protein-based surfactant agent, with cement, ground granulated blast furnace slag, and metakaolin as binders and hemp shiv as natural aggregates. The effect of several parameters is studied, including elaboration method (direct and preformed), amount of pozzolanic additions (0% and 30 of cement weight%), and incorporation of hemp shiv (5 and 15 vol%) on the resulting physical properties, microstructure, porous structure and mechanical behavior of the concrete. Pozzolanic additions improve slightly the uniformity of pore sizes, which increases the mechanical resistance, especially at 28 days. While hemp shiv incorporation results in increased concrete porosity and air bubble radius, it also decreased uniformity, mechanical strength, and lower cohesion with the cement matrix compared to standard concrete. The results contribute to the development of eco-friendly construction materials and promote the utilization of agricultural waste in the construction industry.

Keywords: porous structure; foamed concrete; hemp shiv; biobased materials; mechanical strength

Citation: Mohamad, A.; Khadraoui, F.; Chateigner, D.; Boutouil, M. Influence of Porous Structure of Non-Autoclaved Bio-Based Foamed Concrete on Mechanical Strength. *Buildings* **2023**, *13*, 2261. https://doi.org/10.3390/buildings13092261

Academic Editors: Marco Di Ludovico and Mohamed K. Ismail

Received: 27 June 2023
Revised: 25 July 2023
Accepted: 22 August 2023
Published: 6 September 2023

1. Introduction

Concrete can be categorized based on its density into three main types: conventional, heavyweight, and lightweight. Conventional concrete, also known as standard concrete, is the most used type with a density of 2400 kg/m^3 [1]. It typically contains traditional mineral aggregates such as gravel, sand, and crushed stone. Conventional concrete finds widespread applications in various construction projects, including buildings, bridges, pavements, and foundations. Heavyweight concrete, characterized by a high density greater than 2600 kg/m^3 [1] and can arrive at 3850 kg/m^3 [2], incorporates heavy aggregates such as iron ore, magnetite, or barite. This type of concrete offers exceptional durability, excellent fire resistance, and high mechanical properties. It finds applications in specialized sectors, including nuclear power plants, radiation treatment facilities, and counterweights for structures [1].

Lightweight concrete, on the other hand, is divided into three sub-types: Lightweight aggregates, aerated and foamed concrete. All types of lightweight concrete are widely used in the construction industry because of their many advantages. Foamed concrete (FC) is a mineral matrix incorporating air or gas bubbles. FC is generally designed to achieve a low density of between 400 and 1850 kg/m^3, a very low thermal conductivity compared to usual concretes (from 0.06 to 0.66 W/mK), and a low compressive strength of about 1–30 MPa [3]. Furthermore, Foamed concrete provides other advantages, such

as reduced construction costs, production of lightweight and environmentally friendly structures, sound insulation, and fire resistance [4–8].

There are two mechanical processes to elaborate foamed non-autoclaved concrete (Figure 1). On one hand, the preformed foaming method (Preformed Foam) uses an agent to generate foam before addition to the mineral mix, an adequate technique to produce foamed concrete with high porosity and stable air bubbles [9]. On the other hand, the direct mixing method (by mixing) consists of generating air bubbles directly in the mineral matrix by adding and mixing the foaming agent directly into the cement paste [10]. Numerous research studies have focused on examining the performances and pore characteristics of FC by incorporating additives such as fly ash (FA) and ground granulated blast furnace slag (GGBFS), which are industrial by-products recognized for their eco-friendly and sustainable properties [11,12]. Furthermore, FA and GGBFS have been utilized as substitutes for cement in the production of foam concrete [13,14]. Also, polypropylene [15] and natural [16] fibers have been used to reinforce the foam concrete. While previous studies have explored the influence of incorporating hemp shives, there is still a need to further investigate and expand upon this research area due to its significant potential [17].

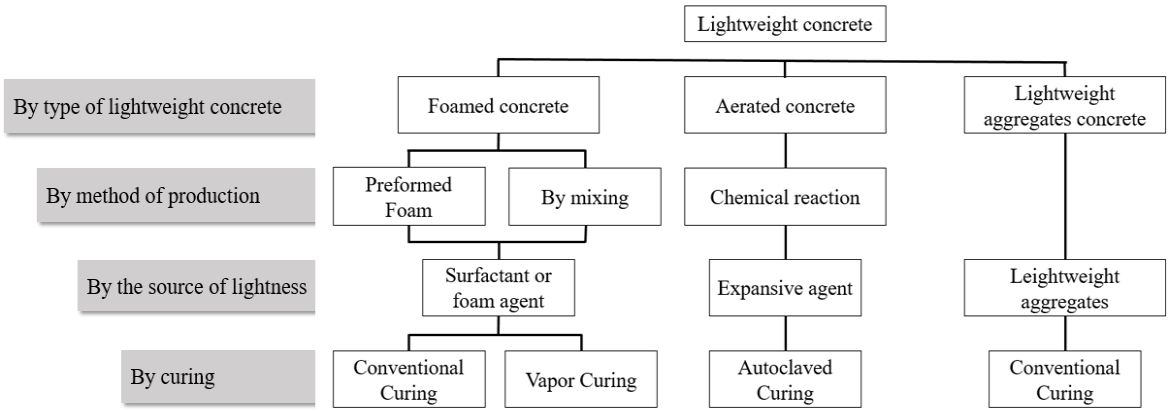

Figure 1. Flowchart of the different types of lightweight concretes.

Usually, hemp shives are used as an alternative to aggregates. For instance, Sáez-Pérez et al. [18] that hemp concrete serves dual purposes as both a construction material and an insulation material. The valuable characteristics of hemp concrete are its lightweight, highly porous structure, low thermal conductivity, excellent moisture buffer capability, and acoustic insulation, all allowing reduction of building energy consumption [19–21]. Also, biogenic materials are playing an increasingly important role in the composition of building materials [22,23].

The characterization of air-voids in foam concrete can be achieved by considering several parameters, including volume, radius, distribution, shape, and spacing between voids [3]. The porosity and the air bubbles structure appear to condition the thermal conductivity and mechanical properties of foam concrete [24]. For instance, Kearsley et al. proved on the one hand that the air-void distribution is one of the most important micro properties influencing the strength of foam concrete, and on the other hand that foam concrete with narrower air-void distributions exhibits higher strengths [25]. Visagie et al. [26] have shown that an increased total porosity (ϕ) in foamed concrete can have a significant negative impact on its compressive strength, particularly when the pores are larger in size. Similar to traditional cementitious materials, foam concrete consists of distinct pore categories, including nano-pores (also known as gel pores) with a diameter less than 0.01 µm, capillary or micropores ranging from 0.01 µm to 10 µm, and macro-pores exceeding 10 µm in diameter.

The addition of GGBFS enhances mechanical strength. Moreover, a study on the air-void system of foamed concrete shows that the incorporation of GGBFS led to a high strength-to-weight ratio [27,28]. The strength of foam concrete is influenced by several

additional parameters, including the cement-to-sand ratio, water-to-cement ratio, curing regimen, type of sand, the particle size distribution of sand, and the choice of foaming agent [29,30]. When aiming for a dry density range of 500 to 1000 kg/m^3, the compressive strength tends to decrease as the diameter of the voids increases. However, for densities exceeding 1000 kg/m^3, where the air voids are more widely spaced and the composition of the concrete mix becomes a more significant factor [31].

The importance of the pore structure on the performances of foamed concretes guided us to explore in the present work the physical properties of pore structure relationship in foamed concretes, especially with the presence of hemp shiv particles. The pore structure is characterized using surface characterization techniques based on image analysis which allows us to carry out the first observations of the alveolar distribution of air bubbles. The relationships between hemp shiv quantity, elaboration process, and their influences on pore structure and associated mechanical performances are described.

2. Materials and Methods

2.1. Raw Materials

The raw materials used for producing FC are:

(i) CEM I 52.5N, which fulfils all the specifications of EN 197-1 Portland cement Type 1.
(ii) Ground Granulated Blast Furnace Slag (GGBFS), which complies with I.S EN 206-1, as a by-product of iron production.
(iii) Metakaolin (MK) is obtained by flash calcination of kaolinite at approximately 700 °C.
(iv) biomass consisting of 95% hemp shives (HS) and 5% hemp fiber, hemp shives are considered renewable raw materials to reduce cost and CO_2 emissions.

A low water/binder ratio and an optimized granular density of the binder matrix would lead to a very solid cementitious matrix, constituting the interface between the air bubbles. Pozzolans are used to increase resistance to sulfate attack and durability, and to reduce CO_2 emissions due to cement and heat of hydration [32,33]. Therefore, GGBFS and MK are used in this study (Table 1).

Table 1. Chemical composition of binder components.

Components	Unit	CEM I	GGBFS	MK
Calcium oxide (CaO)	Weight %	64.17	43	0.2
Aluminum oxide (Al_2O_3)		4.44	10.7	24.1
Silicon dioxide (SiO_2)		19.6	37.3	68.1
Ferric oxide (Fe_2O_3)		4	0.2	3.7
Sulfur trioxide (SO_3)		2.6	0.1	-
Sodium oxide (Na_2O)		0.07	0.23	0.1
Magnesium oxide (MgO)		1.25	6.5	0.2
Potassium oxide (K_2O)		0.84	0.35	0.4
Absolute density	(kg/m^3)	3100	2900	2500

In order to achieve a desirable workability of the mixture while maintaining a low water-to-cement (W/C) ratio, a superplasticizer consisting of polycarboxylate and modified phosphonates is added to each sample. This addition serves to reduce the required water content while ensuring optimal fluidity and workability of the fresh mixture. To produce a more stable bubble network, a commercial foaming agent is used with a foam density of about 70 kg/m^3. The foaming agent used in foam concrete can slow down the hardening process. To overcome this, a setting accelerator is utilized to promote cement hydration, stabilize air bubbles, and accelerate the development of mechanical strength. Also, in order to ease the demoulding of foam concrete after hardening, a demoulding agent is used, whose composition does not contain solvents, to form an anti-adhesive film on the surface of the mould. The characteristics of the superplasticizer, accelerator, and foaming agent are given in Table 2.

Table 2. Properties of admixtures used in this study.

	Accelerator	Superplasticizer	Foam Agent
Color	Yellow	brown	bright yellow
Absolute Density (g/cm^3)	1.45 ± 0.01	1.055 ± 0.01	1.04 ± 0.02
Recommended weight	1–1.5%	1–3%	-
Chlorides content	≤0.1%	≤0.1%	0.001%
pH	6 ± 1	6 ± 1	9
Dry Content (%)	61.5% ± 2.7%	30.5% ± 1.5%	30%

2.2. Specimens Elaboration

A total of eight foam concrete samples were prepared, four using the preformed and four using the direct methods.

The preformed foam method involves separately producing a stable aqueous foam and a mineral suspension, which are later mixed together. The foam is created by combining a diluted foaming agent with water in a 1:30 ratio (by weight). Meanwhile, the powdered constituents and hemp shives are mixed dry in a mortar mixer with a capacity of approximately 20 L. Water, along with the accelerator agent and superplasticizer, is then added to the mixture, which is stirred until a homogeneous paste is achieved. Finally, the mineral suspension is gradually added to the foam and thoroughly stirred at high speed until a homogeneous mixture is obtained.

The direct method, on the other hand, involves adding the foaming agent directly to the mineral mixture after its formation. The preparation of the mineral mixture remains the same in both methods.

In both approaches, the resulting concrete is fluid and foamy, and it is placed into parallelepiped moulds (4 × 4 × 16 cm^3) without any vibration. After 48 h of curing at 20 °C, the samples are demoulded and stored in a damp room with a temperature of 20 °C and relative humidity above 95%. Six 4 × 4 × 16 samples are used to study the mechanical behavior (in compression and flexion) at 7 and 28 days, the other three provide an analysis of the distribution of air bubbles.

Two control foam concrete formulations are used (Table 3), C100H0 and C70H0 (in CxHy, x represents the weight percentage of cement and y the wt% of cement replaced by hemp shiv). Also, in order to specify the method used, D or P are added to the sample name for "direct" and "preformed" methods, respectively.

Table 3. Compositions of formulations studied.

Mixes Names	Fresh Density (kg/m^3)	Composition of Mixture (kg/m^3)							Wt/L
		CEM I	GGBFS	MK	HS	SP	Acc	FAG	
C100P0H0P	891	700	-	-	-	14	7	2.1	0.24
C100P0H0D	1600	1200	-	-	-	24	12	2.1	0.24
C70P30H0P	933	490	140	70	-	7	7	2.1	0.31
C70P30H0D	1589	840	240	120	-	12	12	2.1	0.31
C65P30H5P	900	455	140	70	2.2	6.7	6.7	2.1	0.32
C65P30H5D	1542	780	240	120	3.8	11.4	11.4	2.1	0.32
C55P30H5P	834	385	140	70	6.7	6.1	6.1	2.1	0.34
C55P30H5D	1227	660	240	120	11	10.3	10.31	2.1	0.34

The high water absorption capacity of hemp particles, amounting to approximately 250% of their mass, leads to a competition for water between the hydration of mineral binders and the water absorption of hemp shives [34,35]. This phenomenon results in the chalking of hydraulic binders at the interface between the hemp particles and the binder [36]. Consequently, to mitigate this effect, the water content in different formulations is carefully adjusted in accordance with the volume of hemp shives.

2.3. Methods

The measurement of fresh density follows the NF EN 12350-6 standard [37], where a one-litre container is used with a measuring error of 20 kg/m^3. Dry bulk density is determined following the NF EN 12390-1 standard [38], involving the drying of a group of three 4 × 4 × 16 specimens at 60 °C until a constant weight is achieved. The weight-to-volume ratio is then used to determine the density.

For the measurement of absolute density, ASTM B923 [39] recommends using the AccuPyc II 1340 helium pycnometer. (Micromeritics, Norcross, GA, USA) This instrument accurately measures the volume of the solid phase of a sample with a known weight, providing a reliable measurement of absolute density.

After 7 and 28 days, a parallelepiped specimen is broken in 2 halves by bending and the compressive strength is measured on both halves. The load velocity is 0.05 kN/sec. A universal press (IGM® 250KN press, Magny-les-Hameaux, France) is used to determine the compressive strength *Rc* and the bending strength. These tests are controlled by adapting the standards EN 679 [40] and EN 196 [41]. The thermal conductivity at 7 and 28 days is measured by an HFM 436 Lambda flowmeter (NETZSCH, Selb, Germany) in accordance with EN 12667 standard [42].

The images obtained by the microscope (Keyence Bois-Colombes, France) allow a first observation of the pore structure (Figure 2). It is necessary to use image analysis software to study the distribution of air bubbles and hemp shives. For this purpose, the ImageJ software is used first to determine the surface contribution of the hemp shives and remove it. Then, (Figure 3) the (x, y) positions of the air bubbles are determined on the sample surface, together with their perimeter, surface, small and large radius of the ellipse, and sphericity, by applying several image treatments and analyses (Figure 4). However, it is sometimes difficult to differentiate between two porous structures or to extract quantitative elements to compare them; for this purpose, the use of coal powder to fill the air bubbles is necessary.

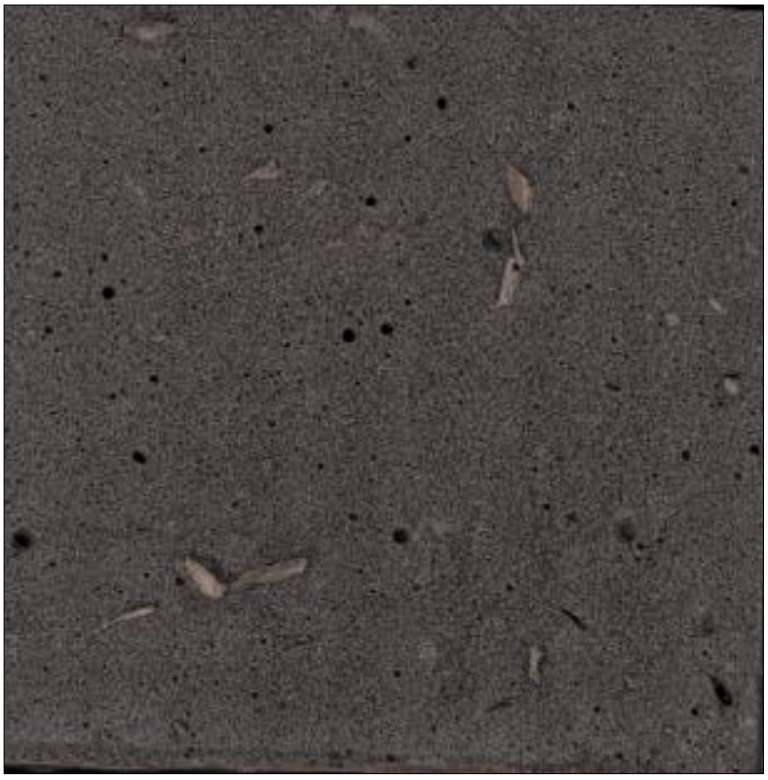

Figure 2. Raw image of the bio-based foamed concrete. Image size is 10,000 × 10,000 pixels.

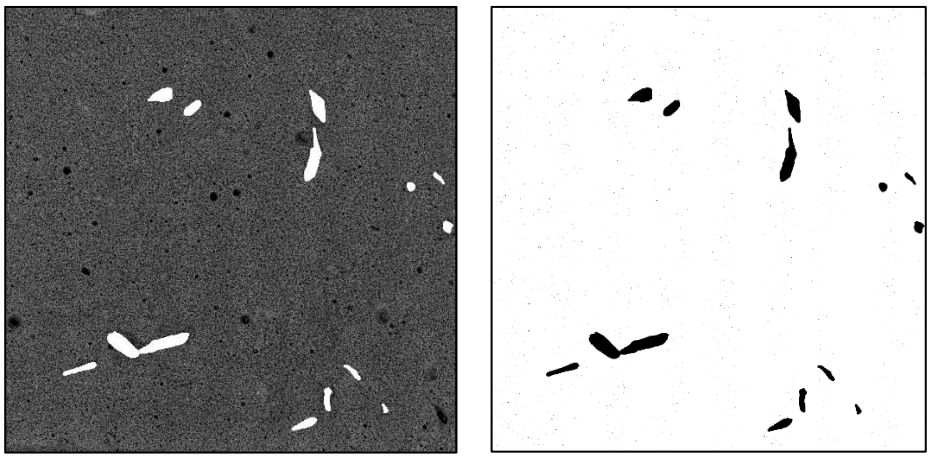

(**a**) (**b**)

Figure 3. Calculation and elimination of the amount of hemp shives. Image size is 10,000 × 10,000 pixels. (**a**) We paint the hemp shiv particles in white (**b**) calculate the area of hemp shiv particles.

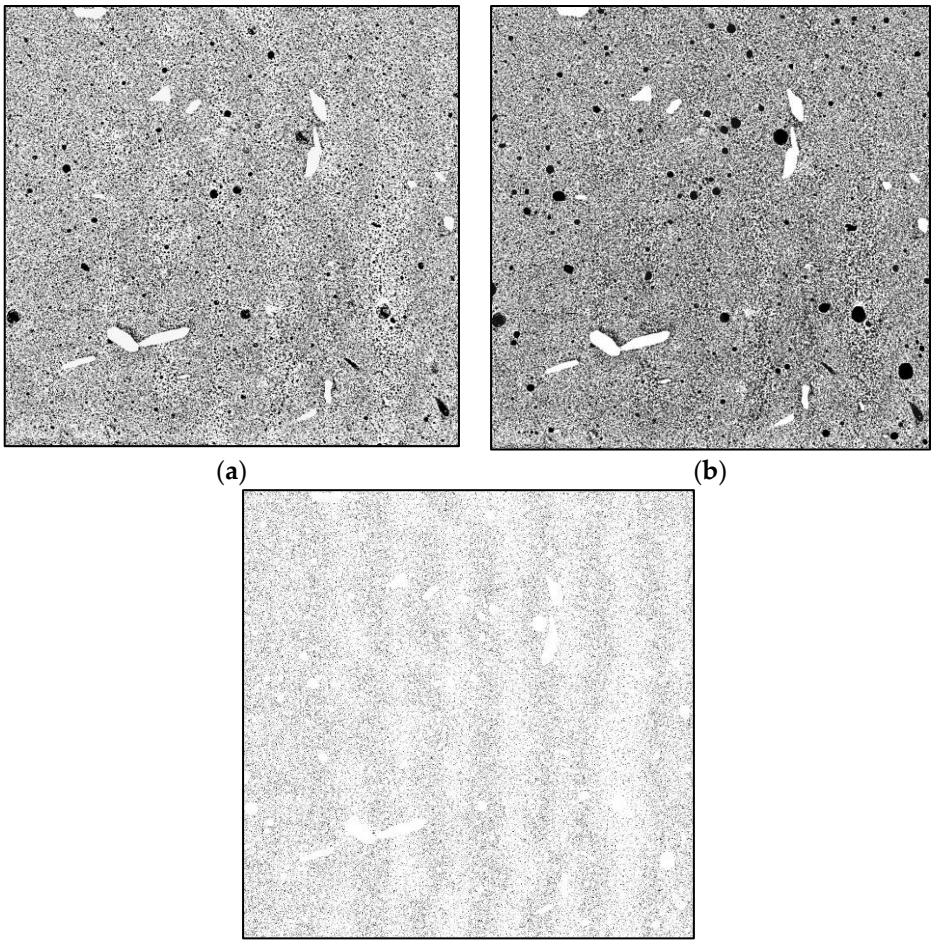

(**a**) (**b**)

(**c**)

Figure 4. Image treatment steps using Image J: (**a**) Contouring of the individual cells; (**b**) Removal of HS reflections and air bubbles detection and coloring (black); (**c**) Edge detection analysis assuming ellipsoidal contours.

3. Results and Discussion

The parameters studied in this work include the quantity of cement and its substitution ratio by hemp aggregates. The density, porosity, compressive and flexural strengths,

and porous structure of the different types of foamed concrete and their mutual effects are evaluated.

3.1. Physical Properties

The performances of foamed concrete, including mechanical strength, thermal conductivity, water resistance, and durability, are primarily influenced by its porosity. Foamed concrete has a higher level of porosity than ordinary concrete. This increased porosity is attributed to the foaming process, which introduces air voids into the concrete mix. As a result, there are more closed and connected pores in the structure of foamed concrete [27]. The porosity is determined by the amount of foam, water, admixtures, and hemp shives present in the formulation. In accordance with the NF EN 1097-6 standard, [43] the total porosity can be obtained by applying the following equation, which utilizes both the absolute density and the bulk density measurements:

$$\Phi = (1 - \frac{\rho_{bulk}}{\rho_{abs}}) \times 100$$

ρ_{bulk}: Bulk density (kg/m^3)
ρ_{true}: Absolute density (kg/m^3)

The bulk densities of the preformed samples range from 579 kg/m^3 to 710 kg/m^3 (Table 4) with a large total porosity from 70.7% to 74.5% while the samples elaborated using the direct method exhibit bulk densities in the 1092–1617 kg/m^3 total porosity in the 32.2–54.6% ranges respectively. The lower total porosity observed in foamed concrete produced by the direct method can be attributed to the direct formation of air bubbles within the mineral suspension, which applies high pressure on their surfaces [44]. In contrast, when using preformed foams, air initially enters the water to generate the foam, and then the mineral suspension is added. During the mixing process at a high rotation speed, the air trapped in the foam remains within the cementitious matrix, resulting in the formation of foamed concrete. It is important to note that controlling air bubble production involves various factors such as rotation speed, mixing time, and directions, which have been maintained constant in this study.

Table 4. Physical properties of the biobased foamed concrete.

Sample	Days	ρ_{bulk} (kg/m^3)	ρ_{true}	Porosity (%)
C100H0P	7 28	710 699	2444	71.4
C100H0D	7 28	1460 1454	2444	40.5
C55H15P	7 28	579 608	2361	74.2
C55H15D	7 28	1092 1083	2361	54.1
C65H5P	7 28	597 662	2381	72.2
C65H5D	7 28	1565 1574	2381	33.9
C70H0P	7 28	690 691	2384	71.0
C70H0D	7 28	1617 1601	2384	32.8

The comparison of the density and porosity of C55H15P, C65H5P, and C70H0P samples (Table 4) shows that sample porosity increases with the increase of hemp shives. This

appears as a coherent behavior since hemp shives exhibit a very low absolute density compared to cement, 140 kg/m^3 and 3100 kg/m^3 respectively.

Table 2 demonstrates that the absolute density of pozzolanic admixtures is slightly lower than that of cement. However, when comparing the total density in Table 4, it is observed that C100H0D (foamed concrete with 100% cement content and no hemp) has a lower density than C70H0D (foamed concrete with 70% cement content and no hemp). This can be explained by the fact that the direct method of foamed concrete production is relatively challenging to control. It depends on various parameters, including mixing time, mixing speed, quantity of surfactants, water quantity, and the constituents of the formulation [3]. These factors can influence the overall density of the resulting foamed concrete and lead to variations in density between different compositions.

For all the elaborated foams the porosity-density relationship evolves linearly (Figure 5). A linear fit of this latter indicates a very similar slope for both direct and preformed elaborated samples.

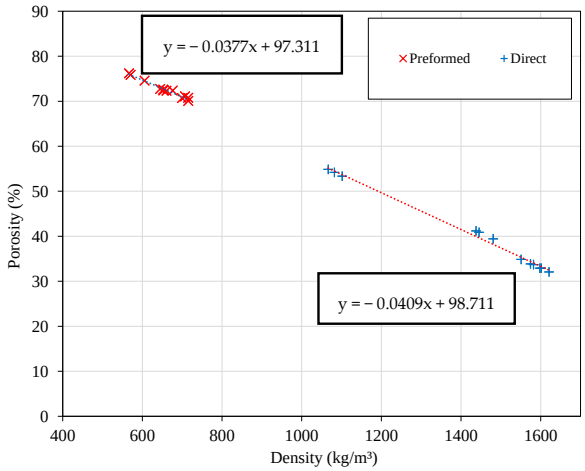

Figure 5. The porosity of all samples against bulk density.

3.2. Pore Size Distributions and Resulting Mechanical Strength

We operated image analysis to evaluate the pore surface distributions of the samples. The homogeneity of the distributions was verified using measurements operated on 3 different sections for each sample (Figures 6 and 7). Whatever the measured section, the pore distributions peak for their maximum at 0.08 mm radius pores (Figure 6), corresponding to a partial area around 45–50% of the apparent total pore section.

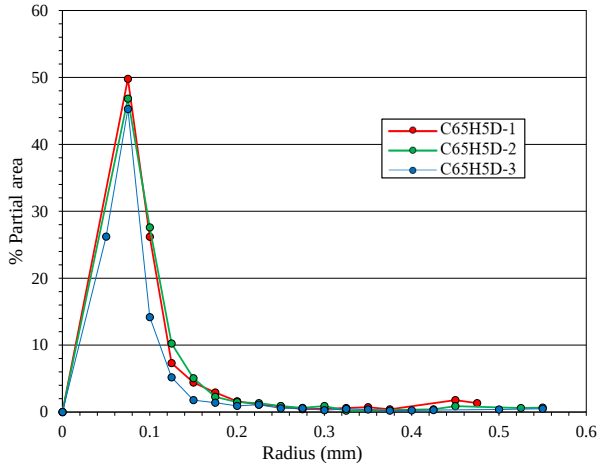

Figure 6. Pore distributions for the three C65H5D sections.

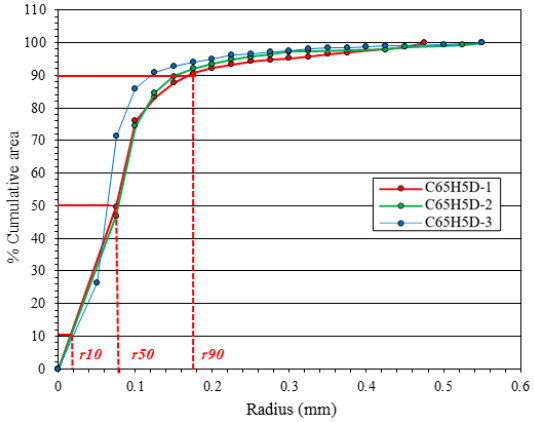

Figure 7. Cumulative pore-size distribution for the three sections of C65H5D.

3.2.1. Influence of Pozzolanic Additions on Pore Distribution

We illustrate the effects of cement replacement by pozzolanic additions (Table 5) on the pore-size distribution of BFCs, comparing one sample without pozzolan addition (C100H0) to one with 30% addition (C70H0 with 20 wt% of GGBFS and 10 wt% of MK). Each sample is elaborated using the two methods, without HS addition. From image analysis, the mean pore radius *(Rm)*, their pore-size-distribution (PSD), and the uniformity coefficient *(UC)* of the samples provide a macroscopic measure of pozzolan addition effects (Table 5 and Figure 8). In the literature, pore-size distribution is considered uniform if $UC = r90/r10 = 1$, with a decreasing homogeneity for increasing *UC* ratio [27].

Table 5. Uniformity Coefficient *(UC)* and mean pore radius *(Rm)* as a function of the mass % of pozzolans *(%PZ)* for the two-elaboration method.

		Preformed		**Direct**	
Sample	***%PZ***	***UC***	***Rm* (mm)**	***UC***	***Rm* (mm)**
C100H0	0	8.41	0.242	9.73	0.153
C70H0	30	5.1	0.188	8.1	0.088

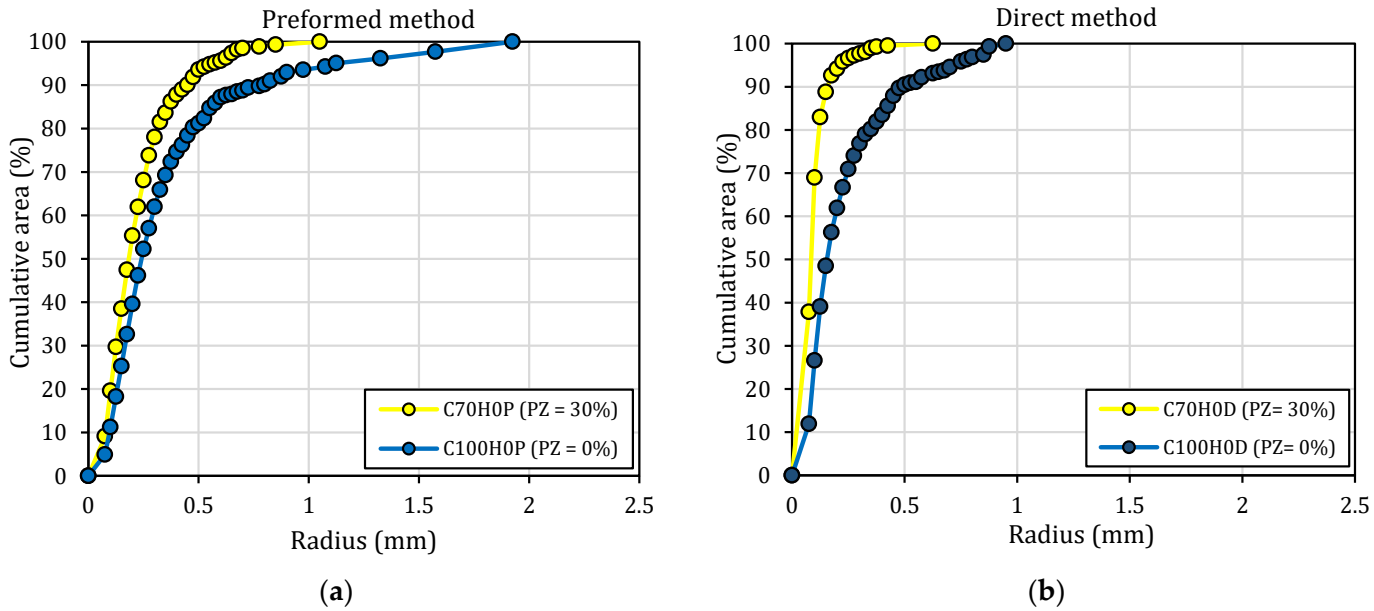

Figure 8. Cumulative pore fraction versus their radius for the two pozzolan fractions: (**a**) preformed and (**b**) direct methods.

However, in our samples, the *UC* parameter is a too restrictive view of the homogeneity. Indeed, while *UC* values (Table 5) seem to indicate weaker pore-size homogeneity using the direct method, comparing the pore-size fraction distribution curves (Figure 8), one can clearly see that the direct method provides samples exhibiting much steeper step-like curves than the preformed method, pointing for a larger size homogeneity in the former. These apparently contradictory observations are explained by the large variability of *UC* estimation on very steep curves, and by the weakness in representing distributions using only a single number *(UC)*. For instance, C100H0P and C70H0D samples which exhibit similar *UC* values but different mean pore radius (Table 5) show very different pore-size distributions (Figures 8a and 8b respectively).

Nevertheless, the distribution curves for samples with 30% pozzolanic additions are steeper than the ones without pozzolanic additions for both methods, and pozzolanic additions give rise to smaller *UC*s, both indicators pointing to more pore-size uniformity upon pozzolan additions. This larger uniformity is accompanied by a mean pore-size decrease, from 0.242 to 0.188 and 0.153 to 0.088 in the preformed and direct methods, respectively. One can also observe that the mean pore-size decrease due to pozzolan addition is more efficient using the direct than using the preformed method, with *Rm* being 57% and 77% of their value without addition, respectively.

The pore-size refinement upon pozzolan additions is also visible directly from microscopic images (Figure 9, compare Figure 9a,c to Figure 9b,d images). The main effect of pozzolanic additions is to ensure cohesion between particles and fill voids which blocks the coalescence of pores, resulting in their smaller size and larger uniformity, also reflected in the PSD (Figure 8) as smoother curve evolutions for C70HO samples. This smoothing effect is observed by the disappearance of large pores (Figure 9c) giving rise to the angular variations of the PSD around 0.5 mm radii (Figure 8b) upon pozzolan addition (Figure 9d).

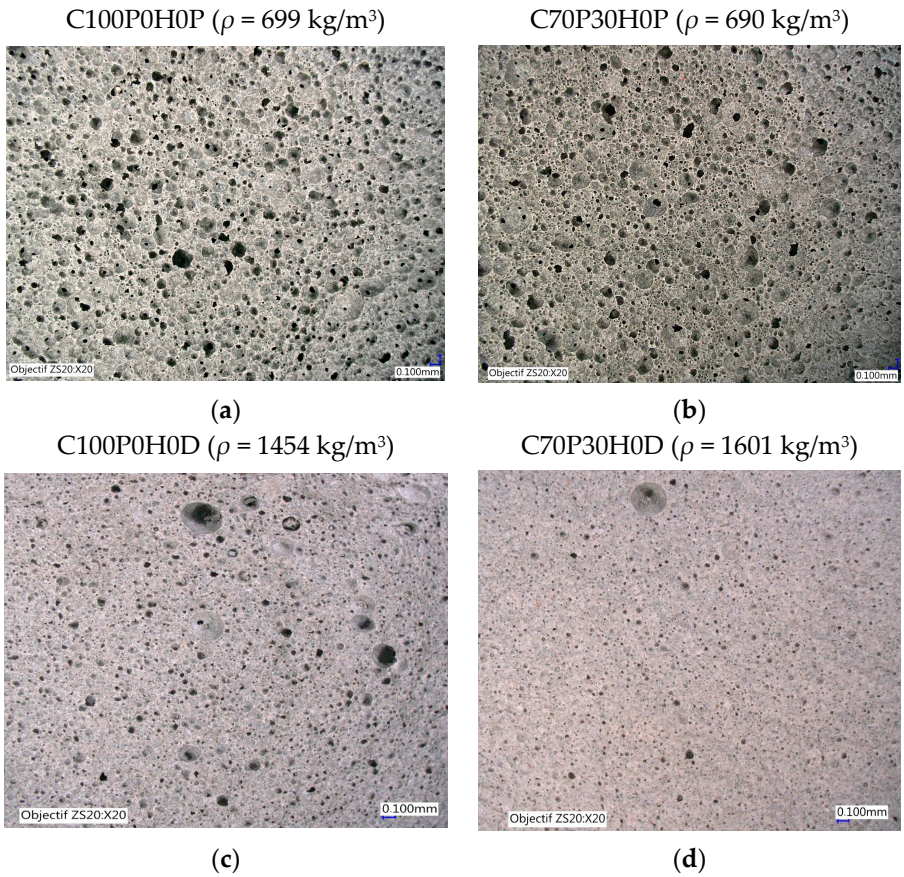

Figure 9. Microscopic images of the porous microstructures of preformed (**a**,**b**) and direct (**c**,**d**) method samples with (**b**,**d**) and without (**a**,**c**) pozzolanic additions.

The observed PSD steepness differences between the two elaboration methods are due to the foaming capacity, the preformed method having a larger capacity to generate pores than the direct method, as seen from the more than 2 times smaller density of the formers.

3.2.2. Influence of Hemp Shiv on Pore Distributions

Hemp shives incorporation in the samples affects their density and consequently obtaining a more detailed picture of their porosity is of major importance.

Using the preformed method (Figure 10a), incorporation of up to 15% hemp shives in 30% pozzolan BFCs does not severely affect the distribution of pores. Only a slight tendency toward larger pore-size ranges is observed. This is reflected by an increase of both *UC* and *Rm* values of 27% and 11% respectively up to 15%HS addition (Table 6).

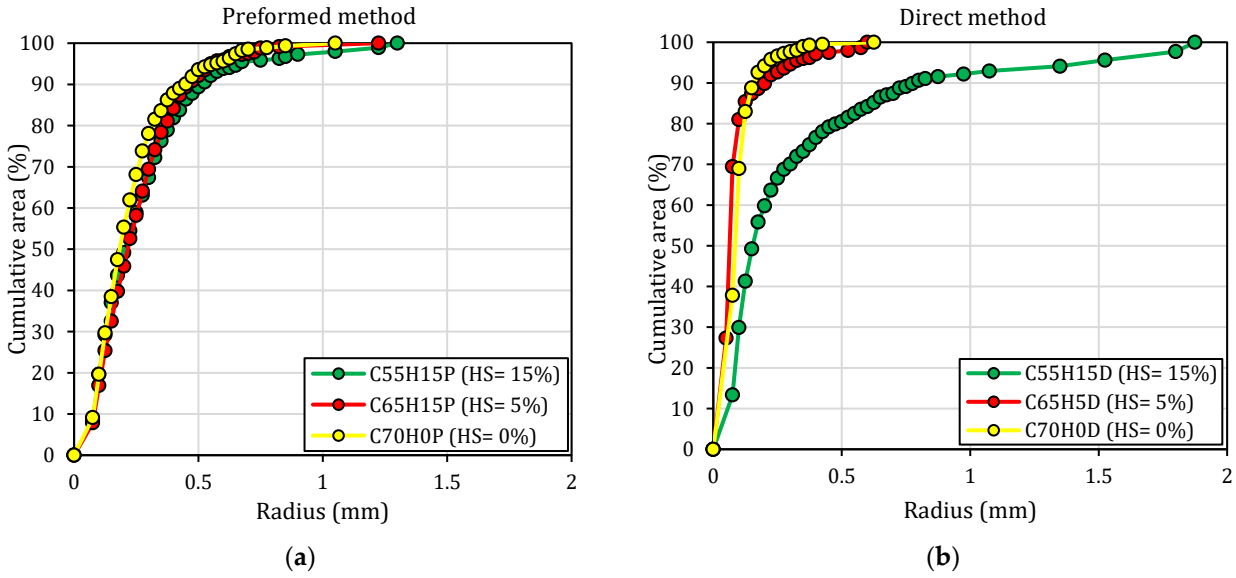

Figure 10. Cumulative pore area versus radius of BFCs incorporating various amounts of hemp shiv (HS) using: (**a**) preformed method, (**b**) direct method.

Table 6. Uniformity Coefficient *UC* and the mean radii *Rm* as a function of the volumic % of hemp shiv *(%HS)*.

		Preformed		**Direct**	
Mixe	**%*HS***	***UC***	***Rm* (mm)**	***UC***	***Rm* (mm)**
C70H0	0	5.1	0.182	8.1	0.088
C65H5	5	5.79	0.219	11.33	0.063
C55H15	15	6.48	0.2	13.52	0.151

Using the direct method (Figure 10b) pore distribution and mean pore radii are also only slightly modified upon hemp shiv addition up to 5%. However, for larger hemp shiv contents (HS = 15%), the pore distribution is skewed towards larger sizes, giving rise to larger *UC* and *Rm* values, the latter reaching twice the value without hemp shiv addition.

Optical microscopy images of the porous structures evidence their invariance upon hemp shiv addition using the preformed method (Figure 11). Whatever the HS content, pore sizes and distribution are constant and hemp shiv is coherently integrated into the BFC matrix with no visible interface between HS and the matrix at these magnifications. Using the direct method (Figure 12), large pores are developed upon HS addition, via pore coalescence, and consequently, both *UC* and *Rm* are increased by a factor of nearly 2. However, in this case, contrary to the preformed samples, a low cohesion between the hemp shives and the cement matrix is observed and results in a larger pore size distribution [34,45]. This decrease in pore size uniformity may consequently affect the mechanical resistance.

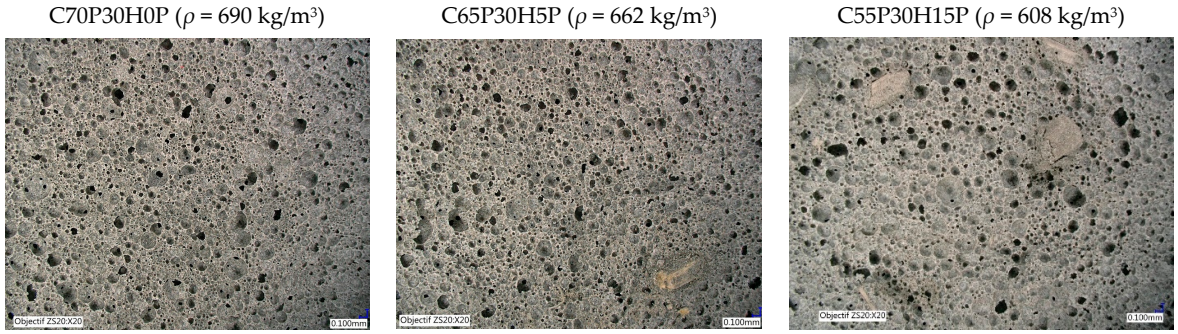

Figure 11. Microscopy images of porous structure evolution with increasing amount of hemp shiv using the preformed method.

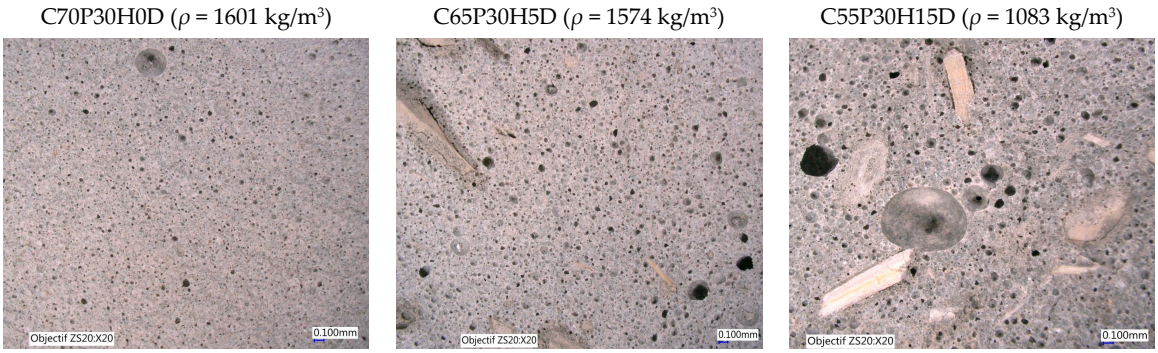

Figure 12. Microscopy images of porous structure evolution with increasing amounts of hemp shiv using the direct method.

3.2.3. Influence of Production Process on Pore Distribution

Whatever HS content and pozzolanic additions (Table 7), all BFCs elaborated by the direct method exhibit finer pore distributions and mean radii.

Table 7. Uniformity Coefficient *UC* and the mean radii *Rm* as a function of production methods.

Sample	*Rm* (mm)	*UC*
C100H0P	0.242	9.73
C100H0D	0.153	8.41
C70H0P	0.182	5.1
C70H0D	0.088	8.1
C65H5P	0.219	5.73
C65H5D	0.063	11.33
C55H15P	0.2	6.48
C55H15D	0.151	13.52

These two next paragraphs are not enlightening. The first one does not say more than what was already said in the previous, and the second concerns the influence on mechanical strength. C65H5D and C65H5P refer to two foam concrete compositions with identical formulations but manufactured using distinct production methods. C65H5D is produced through the direct mixing method, while C65H5P is generated using the preformed method. The mean radii *(Rm)* of these compositions differ, with C65H5D exhibiting an *Rm* value of 0.063 mm and C65H5P displaying an *Rm* value of 0.219 mm. The direct method does not produce a light foam with such a low surfactant dosage. Additionally, for all the other foamed concrete as C70H0 and C100H0, the difference in the average radius is significant but for the C55H15D foams, the radii are closer (*Rm* of C55H15P is equal to 0.2 mm while

for C55H15D is equal to 0.151 mm), due to the low uniformity caused by the low cohesion between the hemp shives and the cement matrix.

In the preformed method, the foam is produced by mixing the surfactant and water separately, which is then combined with the mineral suspension. On the other hand, the direct method involves the formation of air bubbles directly in the mineral suspension. Due to the direct formation of air bubbles, the direct method faces more difficulties in achieving a consistent and controlled foam formation. As mentioned in Section 3.1, the size of the air bubble radius has a significant impact on the porosity of the foam concrete. In the direct method, the merging of bubbles becomes more likely at higher foam volumes, leading to a wider distribution of void sizes. This wide distribution of void sizes results in lower strength of the foam concrete [31,46]. Apart from the air-void size and its distribution, the compressive strength of foam concrete is also influenced by the void/paste ratio, spacing of air-voids, and the frequency of air-voids. The shape factor, which characterizes the uniformity of the shape of air-voids, has a negligible effect on strength [46,47]. Therefore, the preformed method, with its higher porosity, leads to lower densities and mechanical strength in foam concrete when compared to the direct method.

3.3. Mechanical Strength

The compressive strength of foamed concretes is largely dependent on age, constituents, porosity, and density [25,48]. In our samples (Table 8), the ratio between *Rc* at 7 days and the one at 28 days increases from 0.54 to 0.74 for the samples elaborated using the preformed method, and from 0.79 to 0.88 for the direct method concretes. This increase is larger than for ordinary concretes for which such a ratio is usually observed around 0.65 and is mainly due to the hardening accelerator used. Moreover, this *Rc7/Rc28* ratio also increases upon the incorporation of HS, as seen in samples C55H15, C65H5, and C70H0, with a ratio of 0.54, 0.58, and 0.69 for the preformed method and 0.79, 0.85 and 0.88 for the direct method respectively. A previous study of the effect of hemp shives on cement hardening [49] that the high alkalinity of cement can degrade lignocellulosic compounds and generate by-products that inhibit the setting and hardening process. Therefore, hemp shives delay concrete's hardening [50]. Additionally to HS incorporation, pozzolanic materials also delay the hydration process and extend the achievement of stabilization over time [32]. Therefore, the evolution of the mechanical strength of concrete foamed with pozzolanic raw materials C70H0 is larger than those without pozzolanic raw materials C100H0 (Table 5).

Table 8. Compressive and flexural strengths of all samples at 7 and 28 days.

Sample	Days	Density (kg/m^3)	*Rc* (MPa)	*Rf* (MPa)
C100H0P	7 28	710 699	2.13 2.88	1.08 1.36
C100H0D	7 28	1460 1454	20.63 25.32	4.25 4.48
C70H0P	7 28	690 691	2.3 3.73	1.23 1.43
C70H0D	7 28	1617 1601	27.53 31.48	6 6.22
C65H5P	7 28	597 662	2 3.44	0.85 1.02
C65H5D	7 28	1565 1574	24.5 28.67	4.43 5.41
C55H15P	7 28	579 608	1.8 3.11	0.84 0.93
C55H15D	7 28	1092 1083	7.05 8.88	2.01 2.2

The mechanical strength is also dependent on the uniformity of pore distributions and their mean radius. Indeed, HS addition in preformed samples, which exhibit fine radius distributions and dense interfaces between HS particles and the matrix, has only a moderate impact on the mechanical resistance, *Rc*'s at 28 days decreasing from 3.73 MPa in C70HOP to 3.11 MPa in C5515P, and *Rf*'s from 1.43 MPa to 0.93 Mpa, respectively.

But HS addition significantly affects the mechanical strengths of the direct method samples, *Rc*'s and *Rf*'s exhibiting a three-fourth and two-third decrease respectively up to 15% HS contents. These findings align with the observations made in Section 3.2, where it was noted that the highest amount of hemp shives (HS) led to lower uniformity in the distribution of pores. Additionally, weaker cohesion between the shives and the cementitious matrix was observed, resulting in the formation of new gaps within the matrix. Consequently, the material exhibited increased brittleness, leading to significantly lower compressive strengths in foam concrete samples containing 15% HS compared to those without HS or with only 5% HS. Similar decreases in compressive strength have been reported by various researchers in the context of biofiber concrete [51–54]. Additionally, Chamoin [19] also found that the compressive strength of hemp concrete increases with the amount of binder in the formulation.

The large difference in compressive strengths in favour of concretes produced by the direct method is mainly an effect due to their larger density (see Section 3.1). Some studies showed an exponential evolution of the compressive strength with density [3,24], and this is also what we observe in our samples (Figure 13).

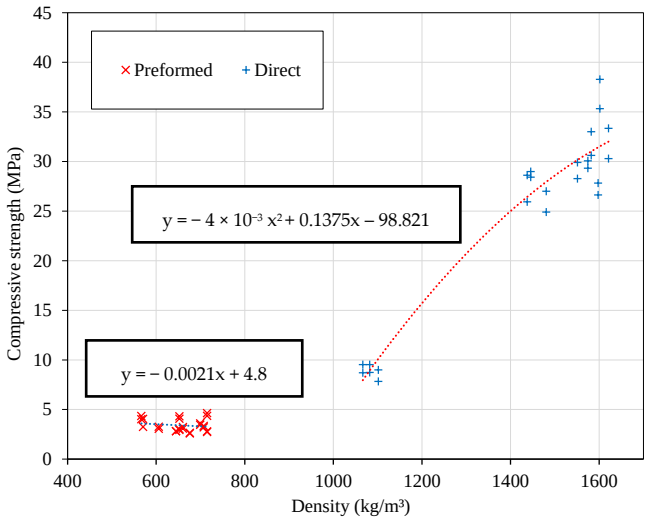

Figure 13. Compressive strength evolution with density at 28-days.

The compressive strength of C100H0D, C70H0D, and C65H5D concretes is larger than 25 MPa, therefore they are considered as structural concretes.

The compressive strength behavior of our samples all lies above 2 MPa. Consequently, even the more porous samples also can be considered as semi-structural bio-based concretes. Therefore, the direct method can be used to produce structural foam concretes and the preformed method to elaborate semi-structural, lighter foam concretes.

The *Rf/Rc* ratio, as presented in Table 8, exhibits a range of 0.15 to 0.25 for the direct method and 0.3 to 0.45 for the preformed method. The difference in these ratios primarily stems from the density of the foamed concrete. Notably, the *Rf/Rc* ratio tends to decrease as the density increases. In the bibliography, in the case of cellular concrete with densities below 1000 kg/m^3, the observed *Rf/Rc* ratio falls within the range of 0.25 to 0.35 [55]. Also, in ordinary concretes it ranges usually between 0.1 and 0.2 [56]. Compared to ordinary, foamed or not, concretes, the addition of HS decreases the flexural strength less than it decreases the compressive strength, thus increasing the *Rf/Rc* ratio. This is the case independently of the chosen elaboration method.

Similarly, as for the compressive strength, the evolution of flexure strength (Figure 14) with density in the foamed concretes exhibits a behavior compatible with an exponential character.

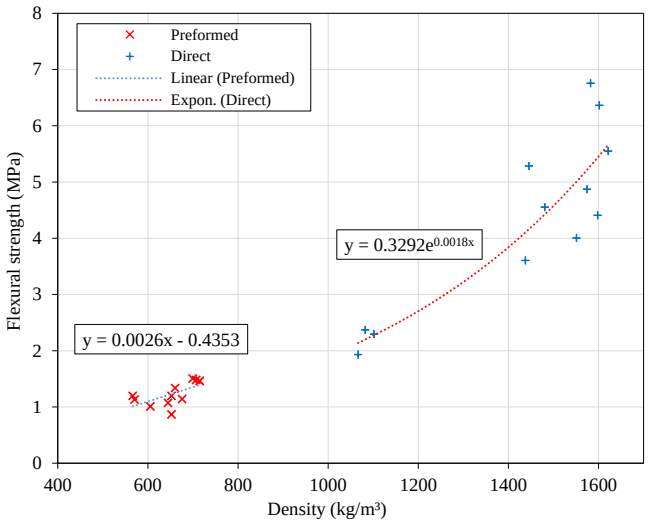

Figure 14. Flexural strength of all samples against density at 28-days.

4. Conclusions

The porous structure of non-autoclaved bio-based foamed concretes manufactured using cement, Ground Granulated Blast Furnace Slags, Metakaolin, pozzolans, and hemp shives, are influencing many sample characteristics. The parameters that define the void network are correlated with the mechanical performances. We can point out the following conclusions:

- Hemp shives increase the porosity and thus decrease the density of the samples. An increase in pore mean radius is observed upon addition, which decreases pore size uniformity and correlatively the mechanical resistance.
- The amount of cement and pozzolanic materials improve slightly the uniformity of pore sizes, which increases the mechanical resistance, especially at 28 days.
- The production method used plays a crucial role in the formation of pores in foam concrete. The preformed method demonstrates higher efficiency in forming foam for lightweight concrete with a density lower than 700 kg/m^3 and achieves a compressive strength of approximately 3.5 MPa. In contrast, the direct method yields foam concrete with finer pores and more uniform pore-size distributions.
- The application of a porous structure characterization technique makes it possible to establish correlations between mechanical performance and the pore structure. The mechanical strength of mineral foams depends mainly on three parameters: porosity, mineral matrix strength, distribution, and size of pores. These four parameters are influenced by the formulation and production method. An analysis of the pore structure shows that a homogeneous distribution of small pores gives rise to the best mechanical performance.
- This study shows that the amount of porosity in foamed concretes is the main microstructural parameter controlling their mechanical properties.

In conclusion, further research should focus on determining the optimum ratio of hemp shives to strike a balance between increased porosity and reduced mechanical strength in non-autoclaved biobased foamed concretes. It is also recommended to study the effect of curing conditions, mixing techniques with other biobased aggregates, and other particle sizes on the pore structure and mechanical properties of non-autoclaved biobased foamed concretes.

Author Contributions: Validation, F.K., D.C. and M.B.; Writing—original draft, A.M.; Writing—review & editing, F.K., D.C. and M.B. All authors have read and agreed to the published version of the manuscript.

Funding: This research received no external funding.

Conflicts of Interest: The authors declare no conflict of interest.

References

1. Khalaf, M.A.; Ban, C.C.; Ramli, M. The constituents, properties and application of heavyweight concrete: A review. *Constr. Build. Mater.* **2019**, *215*, 73–89. [CrossRef]
2. Kukreti, A.; Kundra, P.; Kathait, L.; Garg, N.; Kumar, S. A Review on Properties of Heavy Weight Concrete. *IOP Conf. Ser. Earth Environ. Sci.* **2022**, *1086*, 012049. [CrossRef]
3. Amran, Y.M.; Farzadnia, N.; Ali, A.A. Properties and applications of foamed concrete; a review. *Constr. Build. Mater.* **2015**, *101*, 990–1005. [CrossRef]
4. Priyatham, B.; Lakshmayya, M.; Chaitanya, D. Review on performance and sustainability of foam concrete. *Mater. Today Proc.* **2023**, *17*, 80. [CrossRef]
5. Ramamurthy, K.; Nambiar, E.K.; Ranjani, G.I.S. A classification of studies on properties of foam concrete. *Cem. Concr. Compos.* **2009**, *31*, 388–396. [CrossRef]
6. Kearsley, E.; Wainwright, P. Porosity and permeability of foamed concrete. *Cem. Concr. Res.* **2001**, *31*, 805–812. [CrossRef]
7. Mohamad, N.; Omar, W.; Abdullah, R. Precast Lightweight Foamed Concrete Sandwich Panel (PLFP) Tested under Axial Load: Preliminary Results. *Adv. Mater. Res.* **2011**, *250–253*, 1153–1162. [CrossRef]
8. Zhang, X.; Yang, Q.; Shi, Y.; Zheng, G.; Li, Q.; Chen, H.; Cheng, X. Effects of different control methods on the mechanical and thermal properties of ultra-light foamed concrete. *Constr. Build. Mater.* **2020**, *262*, 120082. [CrossRef]
9. Jiang, J.; Lu, Z.; Niu, Y.; Li, J.; Zhang, Y. Study on the preparation and properties of high-porosity foamed concretes based on ordinary Portland cement. *Mater. Des.* **2016**, *92*, 949–959. [CrossRef]
10. Fabien, A.; Sebaibi, N.; Boutouil, M. Effect of several parameters on non-autoclaved aerated concrete: Use of recycling waste perlite. *Eur. J. Environ. Civ. Eng.* **2019**, *26*, 58–75. [CrossRef]
11. Nath, P.; Sarker, P.K. Effect of GGBFS on setting, workability and early strength properties of fly ash geopolymer concrete cured in ambient condition. *Constr. Build. Mater.* **2014**, *66*, 163–171. [CrossRef]
12. Gholampour, A.; Ozbakkaloglu, T. Performance of sustainable concretes containing very high volume Class-F fly ash and ground granulated blast furnace slag. *J. Clean. Prod.* **2017**, *162*, 1407–1417. [CrossRef]
13. Gökçe, H.S.; Hatungimana, D.; Ramyar, K. Effect of fly ash and silica fume on hardened properties of foam concrete. *Constr. Build. Mater.* **2019**, *194*, 1–11. [CrossRef]
14. Yang, L.; Yan, Y.; Hu, Z. Utilization of phosphogypsum for the preparation of non-autoclaved aerated concrete. *Constr. Build. Mater.* **2013**, *44*, 600–606. [CrossRef]
15. Pretot, S.; Collet, F.; Garnier, C. Life cycle assessment of a hemp concrete wall: Impact of thickness and coating. *Build. Environ.* **2014**, *72*, 223–231. [CrossRef]
16. Amran, Y.H.M.; Alyousef, R.; Alabduljabbar, H.; Khudhair, M.H.R.; Hejazi, F.; Alaskar, A.; Alrshoudi, F.; Siddika, A. Performance properties of structural fibred-foamed concrete. *Results Eng.* **2020**, *5*, 100092. [CrossRef]
17. Sebaibi, N.; Khadraoui-Mehir, F.; Kourtaa, S.; Boutouil, M. Optimization of non-autoclaved aerated insulating foam using bio-based materials. *Constr. Build. Mater.* **2020**, *262*, 120822. [CrossRef]
18. Sáez-Pérez, M.; Brümmer, M.; Durán-Suárez, J. A review of the factors affecting the properties and performance of hemp aggregate concretes. *J. Build. Eng.* **2020**, *31*, 101323. [CrossRef]
19. Chamoin, J. Optimisation des Propriétés (Physiques, Mécaniques Et Hydriques) de Bétons De Chanvre Par La Maîtrise De La Formulation, Thesis, Rennes, INSA. 2013. Available online: http://www.theses.fr/2013ISAR0016 (accessed on 11 October 2018).
20. De Prez, J.; Van Vuure, A.W.; Ivens, J.; Aerts, G.; Van de Voorde, I. Enzymatic treatment of flax for use in composites. *Biotechnol. Rep.* **2018**, *20*, e00294. [CrossRef]
21. Barbhuiya, S.; Das, B.B. A comprehensive review on the use of hemp in concrete. *Constr. Build. Mater.* **2022**, *341*, 127857. [CrossRef]
22. Ezziane, K.; Bougara, A.; Kadri, A.; Khelafi, H.; Kadri, E. Compressive strength of mortar containing natural pozzolan under various curing temperature. *Cem. Concr. Compos.* **2007**, *29*, 587–593. [CrossRef]
23. Sawadogo, M.; Benmahiddine, F.; Hamami, A.E.A.; Belarbi, R.; Godin, A.; Duquesne, M. Investigation of a novel bio-based phase change material hemp concrete for passive energy storage in buildings. *Appl. Therm. Eng.* **2022**, *212*, 118620. [CrossRef]
24. Samson, G.; Phelipot-Mardele, A.; Lanos, C. Structure Porale de Mousses Minérales. In Proceedings of the Rencontres Universitaires de Génie Civil, Bayonne, France, 27–29 May 2015; Available online: https://hal.archives-ouvertes.fr/hal-01167751 (accessed on 11 October 2018).
25. Kearsley, E.; Wainwright, P. The effect of high fly ash content on the compressive strength of foamed concrete. *Cem. Concr. Res.* **2001**, *31*, 105–112. [CrossRef]

26. Visagie, M. The Effect of Microstructure On The Properties Of Foamed Concrete. Ph.D. Thesis, University of Pretoria, Pretoria, South Africa, 2007. Available online: https://repository.up.ac.za/handle/2263/23075 (accessed on 10 July 2020).
27. Chen, L.; Chen, X.; Wang, L.; Ning, Y.; Ji, T. Compressive strength, pore structure, and hydration products of slag foam concrete under sulfate and chloride environment. *Constr. Build. Mater.* **2023**, *394*, 132141. [CrossRef]
28. Hilal, A.A.; Thom, N.H.; Dawson, A.R. On void structure and strength of foamed concrete made without/with additives. *Constr. Build. Mater.* **2015**, *85*, 157–164. [CrossRef]
29. Hamidah, M.S.; Azmi, I.; Ruslan, M.R.A.; Kartini, K.; Fadhil, N.M. Optimisation of Foamed Concrete Mix Of Different Sand-Cement Ratio And Curing Conditions. In *Use of Foamed Concrete in Construction*; Thomas Telford Publishing: London, UK, 2005; pp. 37–44.
30. Aldridge, D. Introduction to foamed concrete: What, why, how? In *Use of Foamed Concrete in Construction*; Thomas Telford Publishing: London, UK, 2005; pp. 1–14.
31. Visagie, M.; Kearsley, E. Properties of Foamed Concrete As Influenced By Air-Void Parameters. *Concr. Beton.* **2002**, *101*, 8–14.
32. E-Beton-Ultra-Leger-Thermolitys.Pdf, (n.d.). Available online: https://www.cerib.com/wp-content/uploads/2017/05/282-e-beton-ultra-leger-thermolitys.pdf (accessed on 13 May 2019).
33. Zerrouki, R.; Benazzouk, A.; Courty, M.; Ben Hamed, H. Potential use of matakaolin as a partial replacement of preformulated lime binder to improve durability of hemp concrete under cyclic wetting/drying aging. *Constr. Build. Mater.* **2022**, *333*, 127389. [CrossRef]
34. Arnaud, L.; Gourlay, E. Experimental study of parameters influencing mechanical properties of hemp concretes. *Constr. Build. Mater.* **2012**, *28*, 50–56. [CrossRef]
35. Nguyen, T.T. Contribution à L'étude de la Formulation et du Procédé de Fabrication D'éléments de Construction en Béton de Chanvre. Ph.D. Thesis, Université de Bretagne Sud, Lorient, France, 2010. Available online: https://theses.hal.science/tel-01017510 (accessed on 17 July 2023).
36. Cerezo, V. Propriétés Mécaniques, Thermiques et Acoustiques d'un Matériau à Base de Particules Végétales: Approche Expérimentale et Modélisation Théorique. Ph.D. Thesis, Institut National des Sciences Appliquées, Lyon, France, 2005.
37. *NF EN 12350-6*; Afnor EDITIONS. AFNOR: Paris, France, 2019. Available online: https://www.boutique.afnor.org/fr-fr/norme/nf-en-123506/essais-pour-beton-frais-partie-6-masse-volumique/fa190562/83423 (accessed on 5 September 2023).
38. *NF EN 12350-1*; Afnor EDITIONS. AFNOR: Paris, France, 2019. Available online: https://www.boutique.afnor.org/fr-fr/norme/nf-en-123501/essais-pour-beton-frais-partie-1-prelevement-et-appareillage-commun/fa190557/83429 (accessed on 5 September 2023).
39. *ASTM B923 ASTM D5550 ASTM D6093*; Pycnomètre à Gaz Professionnel. Industrie Des Produits Qualtech. ASTM: West Conshohocken, PA, USA, 2023. Available online: https://www.qualtechproductsindustry.com/fr/des-produits/instruments-de-test-des-proprietes-physiques/instruments-de-test-de-densite/pycnometre-a-gaz/ (accessed on 5 September 2023).
40. *NF EN 679*; Afnor EDITIONS. AFNOR: Paris, France, 2005. Available online: https://m.boutique.afnor.org/fr-fr/norme/nf-en-679/determination-de-la-resistance-a-la-compression-du-beton-cellulaire-autocla/fa137268/26321 (accessed on 5 September 2023).
41. *NF EN 196-1*; Afnor EDITIONS. AFNOR: Paris, France, 2016. Available online: https://www.boutique.afnor.org/fr-fr/norme/nf-en-1961/methodes-dessais-des-ciments-partie-1-determination-des-resistances/fa184622/57803 (accessed on 5 September 2023).
42. *BS EN 12667:2001*; Thermal Performance of Building Materials and Products. Determination of Thermal Resistance by Means of Guarded Hot Plate and Heat Flow Meter Methods. Products of High and Medium Thermal Resistance. BSI: London, UK, 2001. Available online: https://www.en-standard.eu/bs-en-12667-2001-thermal-performance-of-building-materials-and-products-determination-of-thermal-resistance-by-means-of-guarded-hot-plate-and-heat-flow-meter-methods-products-of-high-and-medium-thermal-resistance/ (accessed on 5 September 2023).
43. *NF EN 1097-6*; Afnor EDITIONS. AFNOR: Paris, France, 2014. Available online: https://www.boutique.afnor.org/fr-fr/norme/nf-en-10976/essais-pour-determiner-les-caracteristiques-mecaniques-et-physiques-des-gra/fa163899/42536 (accessed on 5 September 2023).
44. Samson, G. Synthèse et Propriétés Des Mousses Minérales, Thesis, Rennes, INSA. 2015. Available online: http://www.theses.fr/2015ISAR0015 (accessed on 11 October 2018).
45. Diquélou, Y.; Gourlay, E.; Arnaud, L.; Kurek, B. Impact of hemp shiv on cement setting and hardening: Influence of the extracted components from the aggregates and study of the interfaces with the inorganic matrix. *Cem. Concr. Compos.* **2015**, *55*, 112–121. [CrossRef]
46. Nambiar, E.K.; Ramamurthy, K. Air-void characterisation of foam concrete. *Cem. Concr. Res.* **2007**, *37*, 221–230. [CrossRef]
47. Wee, T.-H.; Babu, D.S.; Tamilselvan, T.; Lim, H.-S. Air-void system of foamed concrete and its effect on mechanical properties. *ACI Mater. J.* **2006**, *103*, 45–52.
48. Kearsley, E.; Mostert, D. Designing Mix Composition of Foamed Concrete with High Fly Ash Contents. In Proceedings of the Inter-National Conference on the Use of Foamed Concrete in Construction, Dundee, UK, 5 July 2005; pp. 29–36.
49. Diquélou, Y.; Gourlay, E.; Arnaud, L.; Kurek, B. Influence of binder characteristics on the setting and hardening of hemp lightweight concrete. *Constr. Build. Mater.* **2016**, *112*, 506–517. [CrossRef]
50. Balčiūnas, G.; Pundienė, I.; Lekūnaitė-Lukošiūnė, L.; Vėjelis, S.; Korjakins, A. Impact of hemp shives aggregate mineralization on physical–mechanical properties and structure of composite with cementitious binding material. *Ind. Crop. Prod.* **2015**, *77*, 724–734. [CrossRef]

51. Sawsen, C.; Fouzia, K.; Mohamed, B.; Moussa, G. Effect of flax fibers treatments on the rheological and the mechanical behavior of a cement composite. *Constr. Build. Mater.* **2015**, *79*, 229–235. [CrossRef]
52. Kriker, A.; Debicki, G.; Bali, A.; Khenfer, M.; Chabannet, M. Mechanical properties of date palm fibres and concrete reinforced with date palm fibres in hot-dry climate. *Cem. Concr. Compos.* **2005**, *27*, 554–564. [CrossRef]
53. Sawsen, C.; Fouzia, K.; Mohamed, B.; Moussa, G. Optimizing the formulation of flax fiber-reinforced cement composites. *Constr. Build. Mater.* **2014**, *54*, 659–664. [CrossRef]
54. Page, J.; Khadraoui, F.; Boutouil, M.; Gomina, M. Multi-physical properties of a structural concrete incorporating short flax fibers. *Constr. Build. Mater.* **2017**, *140*, 344–353. [CrossRef]
55. Valore, R.C., Jr. Cellular Concretes Part 2 Physical Properties. *J. Proc.* **1954**, *50*, 817–836. [CrossRef]
56. Namsone, E.; Šahmenko, G.; Korjakins, A. Durability Properties of High Performance Foamed Concrete. *Procedia Eng.* **2017**, *172*, 760–767. [CrossRef]